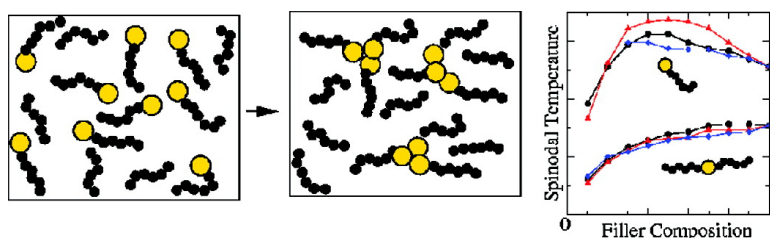Article

Effective Interactions, Structure, and Phase Behavior of Lightly Tethered Nanoparticles in Polymer Melts

Arthi Jayaraman, and Kenneth S. Schweizer

More About This Article

Additional resources and features associated with this article are available within the HTML version:

- Supporting Information
- Access to high resolution figures
- Links to articles and content related to this article
- Copyright permission to reproduce figures and/or text from this article

View the Full Text HTML

Effective Interactions, Structure, and Phase Behavior of Lightly Tethered Nanoparticles in Polymer Melts

Arthi Jayaraman and Kenneth S. Schweizer*

Department of Materials Science and Engineering and Frederick Seitz Materials Research Laboratory, University of Illinois, 1304 West Green Street, Urbana, Illinois 61801

ABSTRACT: We have generalized the microscopic polymer reference interaction site model (PRISM) theory to study the structure and phase behavior of polymer-tethered spherical nanoparticles in a dense homopolymer melt. In the absence of a polymer matrix, fluids of such hybrid nanoparticles show strong concentration fluctuations indicative of aggregate formation and/or a tendency for microphase separation as the total packing fraction and/or nanoparticle attraction strength increase. In the presence of a polymer matrix, there is a competition between tether-mediated microphase separation and matrix-induced macrophase separation. For a single tether of eight segments on a nanoparticle twice the diameter of a segment, the apparent microphase spinodal curve exhibits both dilution-like and depletion-like features and a nonmonotonic dependence of the spinodal temperature on matrix chain length. As the particle size and tether length are both increased, such that the total space filling volume of the tether continues to equal the nanoparticle volume, the shape of the microphase spinodal curve remains unchanged, but the effect of matrix polymer chain length on the spinodal temperature diminishes. For a larger filler, the tendency for macrophase separation grows with increasing matrix polymer length. As the number of tethers is increased, the microphase spinodal curves become more dilution-like, and the effect of matrix degree of polymerization, particle size, and tether length on the apparent spinodal temperature diminishes.

I. Introduction

Polymer nanocomposites[1,2] consist of nanoparticle additives ("fillers") embedded in a polymer matrix. They offer a variety of enhanced thermal, mechanical, optical, and electronic properties relative to pure polymeric materials because of interactions between fillers and the polymer matrix. One of the biggest challenges is the rational control of filler clustering or aggregation, which often adversely affects material properties. In the past few years, several research groups have modified the surface of nanoparticle fillers in an effort to improve their dispersion in a polymer matrix. For example, if nanoparticles are grafted with chains compatible with the matrix polymer, filler dispersion is favored.[3–8] Motivated by this concept, experimentalists have synthesized nanometer and micrometer sized particles with high surface grafting density.[5,9,10] At fixed polymer chemistry, when the molecular weight of matrix polymer is lower (higher) than that of grafted polymer, the nanoparticles disperse (aggregate).[5] More recently, nanoparticles grafted with a relatively small and controlled number of synthetic grafted polymers,[11–14] such as single-tethered CdTe quantum dots,[12] gold nanoparticles with a single PEO tether,[15] and fullerenes end capped with polymethylmethacrylate (PMMA),[16] have been synthesized. Theoretical studies[17–25] have shown that concentrated solutions and melts of this new class of hybrid nanoparticles with low grafting density can indeed assemble into a variety of nanostructures. However, their use as fillers in polymer nanocomposites has been explored very little, and this is the subject of the present theoretical study.

In recent work,[24,25] we generalized and applied the microscopic polymer reference interaction site model (PRISM) theory[26,27] to study concentrated solutions and melts of one-, two-, and four-tethered spherical nanoparticles. The role of tether length, particle size, number and placement of tethers, total packing fraction, and interparticle attraction strength on the real space statistical structure and scattering patterns, and tendency toward aggregation and/or microphase separation, was investigated. We found that strong concentration fluctuations indicative of clustering and/or incipient microphase ordering occur with increasing total packing fraction and/or nanoparticle attraction strength. In analogy with block copolymers,[28] a microphase spinodal curve was deduced by extrapolation of the inverse intensity of the small angle scattering peak. For one-, two-, and four-tethered nanoparticles with a core diameter twice that of the monomer, the microphase spinodal temperature grows roughly as a power law of packing fraction. The apparent scaling law exponent is less than unity and varies with the number of tethers, and the spinodal curve shifts to lower temperatures with increasing number of tethers. We compared our microphase spinodal calculations for single-tethered particles with a recent simulation by Glotzer and co-workers[21] and found the agreement to be surprisingly good. Upon increasing the nanoparticle diameter, the microphase spinodal temperature decreases, and its packing fraction dependence qualitatively changes because of a competition between increased tendency for macrophase separation and decreased tether-induced driving force for microphase transition.

In this work, we study in detail single- and two-tethered spherical nanoparticles in a homopolymer matrix. In this system, there is a competition between tether-induced steric stabilization which can induce microphase ordering, and matrix-induced depletion-like attraction which can drive macrophase separation. For single-tethered nanoparticles, the shape of the microphase spinodal curve is a combination of dilution-like (as in copolymer-homopolymer mixtures[29] or solutions of diblock copolymers[30]) and depletion-like (as seen in colloid-polymer mixtures[31,32]) behavior. Furthermore, the microphase spinodal temperature is a nonmonotonic function of matrix chain length. As the nanoparticle size is increased at a constant tether length, the tendency for macrophase separation increases. As the nanoparticle size and tether length are both increased, keeping the total volume of tethered monomers equal to the volume of the nanoparticle, the shape of the microphase spinodal curve remains unchanged, but the effect of varying matrix polymer length on the spinodal temperature diminishes. As the number of tethers is increased from one to six, the microphase spinodal curves become more dilution-like, and the effect of matrix polymer length, tether

* Corresponding author. E-mail: kschweiz@uiuc.edu.
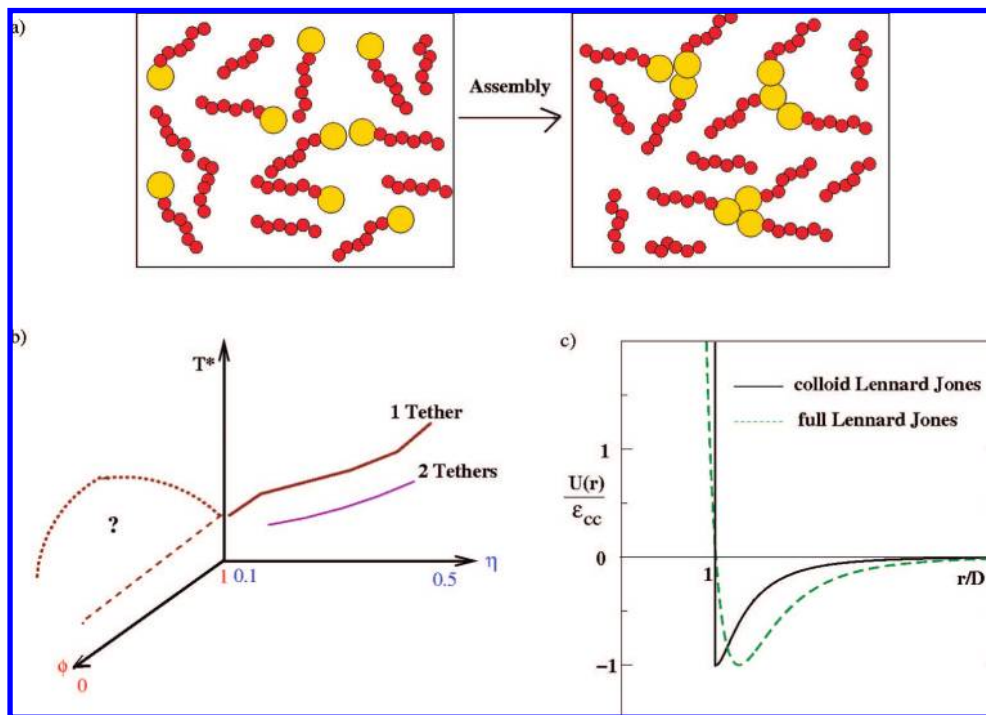
Figure 1. (a) Schematic of the model system containing single-tethered nanoparticles embedded in a polymer melt undergoing cluster formation and higher level ordering. (b) Schematic of the microphase spinodal temperature, T^*, as a function of total fluid packing fraction (η) and filler volume fraction (ϕ). (c) Colloid Lennard Jones potential $U(r)$ (black solid curve) as a function of r/D with $D/b = 2$, and standard Lennard Jones potential (green dashed curve). All potentials are normalized to -1 at the depth of their respective attractive minimum.

length, and particle size on the spinodal temperature is reduced.

The paper is organized as follows. In section II, we discuss the model, theory, and parameters used in this study. A qualitative physical discussion of the homopolymer-mediated competing effects of "depletion" and "dilution" on structure and phase behavior is given in section IIC. Section III presents results for structural correlations in real and Fourier space under purely entropic athermal conditions. In section IV, calculations of local structure, apparent microphase spinodal temperatures, and macrophase separation are given as a function of particle–particle attraction strength. The diverse phase behavior found is interpreted on the basis of the physical discussion presented in section IIC. The paper concludes in section V with a discussion and future outlook. The Appendix collects key formulas required to perform the numerical calculations.

II. Model and Theory

A. Model and Interaction Potentials. The tether and matrix polymer are treated as freely jointed chains (FJC) of N_p and N_m spherical interaction sites (monomers), respectively. The monomers, of diameter d, are connected by a rigid bond of length $l = 1.4 \, d$ (a typical persistence length), where $d \equiv 1$ is the unit of length used throughout the paper. The polymer tethers are permanently grafted on rigid nanoparticle spheres of diameter D. The subscripts p, c, and m denote tether polymer, nanoparticle, and matrix polymer, respectively. The total fluid packing fraction is defined by η, and the fraction of η composed of polymer-tethered particles is the mixture composition variable, ϕ. A schematic of the model system is shown in Figure 1a.

The site–site pair decomposable interactions between tether monomers (or segments), U_{pp}, tether monomers and nanoparticles, U_{pc}, matrix monomers, U_{mm}, matrix and tether monomers, U_{mp}, and matrix monomers and nanoparticles, U_{mc}, all include a hard core repulsion. The only attractive interactions present are between nanoparticles, U_{cc}, modeled beyond contact to be the attractive branch of the colloid Lennard-Jones (CLJ) potential.[33] The CLJ

potential describes the interaction between two nanospheres as a pair wise sum over LJ potentials between elementary units of size b. An example of the attractive branch of the CLJ potential for a polymer-tethered particle with $D = 2b$, where $b = d$, shown in prior work[24] is also given in Figure 1c; its strength is characterized by the value at contact, $-\varepsilon_{cc}$.

Our model system is meant to mimic a polymer nanocomposite composed of tethered nanoparticles dissolved in a homopolymer melt where the matrix and tether polymers are the same chemistry, nanoparticle–homopolymer and homopolymer–homopolymer attractions are weak and very similar, and nanoparticles have a different chemistry from the polymer chains resulting in unbalanced van der Waals attractions between them which can be strong relative to the thermal energy.

B. Polymer Reference Interaction Site Model Theory. PRISM is an equilibrium theory that describes well the structure of both suspensions and dense melts composed of hard spherical particles and linear chains.[24,34−37] The theory is based on the matrix Ornstein–Zernike-like or Chandler–Andersen integral equations[38] that relate the total site–site intermolecular pair correlation function between different sites, $h_{ij}(r) = g_{ij}(r) - 1$, to the site–site intermolecular direct correlation function, $C_{ij}(r)$, and intramolecular probability distribution functions, $\omega_{ij}(r)$. The matrix PRISM equation in Fourier space is

$$\tilde{H}(k) = \tilde{\Omega}(k)\tilde{C}(k)[\tilde{\Omega}(k) + \tilde{H}(k)] \qquad (1)$$

$$H_{ij}(k) = \rho_i\rho_j h_{ij}(k) \qquad (2a)$$

$$\Omega_{ij}(k) = \rho \sum_{\alpha=1}^{N_i} \sum_{\beta=1}^{N_j} \omega_{\alpha i \beta j}(k) \qquad (2b)$$

Here, i and j are two types of interaction sites, N_i is the number of interaction sites of type i, ρ_i the total site density of species i, and ρ is the molecular number density. The 3×3 matrices $\tilde{H}(k)$, $\tilde{C}(k)$, and $\tilde{\Omega}(k)$ describe correlations of three types of sites, c, p, and m; chain end effects are ignored (preaveraged) as in prior applications

of PRISM theory to homopolymers,[26,27] polymer nanocomposites,[34-37] and block copolymers.[39-43] Explicit equations for $h_{ij}(k)$, the tethered nanoparticle $\omega_{ij}(k)$, and the partial collective structure factors, $S_{ij}(k)$, are given in the Appendix. For all calculations, the tethers are attached in fixed positions.

In this initial study, we ignore nonideal conformational perturbations of the tether and matrix polymers. In principle, they can be treated using the fully self-consistent and computationally intensive version of PRISM theory, which involves a medium-induced solvation potential and solution of an effective single-chain problem via Monte Carlo simulation.[27,44] However, the construction and testing of such a solvation potential for tethered particles in a polymer melt is presently an unsolved problem in the framework of PRISM theory. Moreover, we expect chain stretching or contraction effects to be most important in dilute solutions and/or when particle−polymer or polymer−polymer interactions are attractive. Our focus is melt-like packing fractions and polymer-related attractions are absent, conditions where conformational nonidealities of excluded volume and enthalpic origin are expected to be minimized. In addition, we do not consider long tethers, which should also mitigate large nonideal conformational effects, and minimize unphysical intrachain overlaps present in any ideal chain model.[27] We note that, in our previous work[24] on single-tethered particles, on the basis of the same model and statistical mechanical approximations, we demonstrated a surprising good agreement of the predictions of the (estimated) microphase transition with computer simulations for the same hybrid particle model.[21]

Approximate closure relations are required to solve the coupled PRISM integral equations. For polymer nanocomposites (PNC), the site−site Percus−Yevick (PY) closure[26,27,34,37,38] is quite accurate for all direct correlation functions except particle−particle. Previous PNC studies have shown that the hypernetted chain (HNC) approximation[34] is a good closure for the particle−particle direct correlation function, which also ensures the physical condition $g_{cc}(r) > 0$ holds for all r. If σ_{ij} is the distance of closest approach between sites of type i and j, the hard core impenetrability conditions are

$$g_{ij}(r) \equiv 0, \quad r < \sigma_{ij} \tag{3}$$

Outside the hard core, the site−site PY approximation[26,27,34,38] is employed for all, except particle−particle, direct correlations:

$$C_{ij}(r) = (1 - e^{\beta U_{ij}(r)}) g_{ij}(r), \quad r > \sigma_{ij} \tag{4}$$

and the HNC closure[36,45] is adopted for the particle−particle direct correlation function:

$$C_{cc}(r) = h_{cc}(r) - \ln g_{cc}(r) - \beta U_{cc}(r), \quad r > \sigma_{cc} \tag{5}$$

Our prior work[24] for the single tether nanoparticle system demonstrated quite good agreement with simulation,[21] which supports the usefulness of these atomic closures. We note that for polymer blends and block copolymers composed of monomers of (nearly) the same size the so-called "molecular closures" are the most accurate.[27] Whether such closures are better for polymer nanocomposites with hybrid nanoparticles is unknown, and their investigation is beyond the scope of this work.

To efficiently solve the six coupled nonlinear integral equations, we employ the Kinsol algorithm.[46] The Kinsol algorithm is based on the inexact Newton's method and has a relatively high ease of convergence for complex nonlinear integral equations, especially compared with Picard algorithm.[34] Upon solving the PRISM equations, we obtain the pair correlation functions, $g_{ij}(r)$, and partial collective structure factors, $S_{ij}(k)$.

C. Physical Aspects of Filler Dispersion and Phase Behavior. Prior simulation[21] and theoretical work[23-25] has demonstrated that microphase separation can occur for dense solutions of lightly tethered nanoparticles. Earlier work on athermal polymer nanocomposites[36,37,47] has shown that the matrix melt induces a depletion attraction causing macrophase separation of nanofillers. For the case of lightly tethered particles in a polymer matrix, there are potentially three qualitatively different organizational scenarios that can arise because of the competition between nanoparticle-nanoparticle attractions, steric repulsion between grafted tethers, and filler-homopolymer mixing considerations including the depletion-like entropic attraction. (i) Strong intertether repulsions can sterically shield nanoparticle−nanoparticle attractions, and if the depletion effects are weak, then the fillers can form a well-dispersed correlated fluid in the homopolymer matrix. (ii) If intertether repulsion is weak and nanoparticle attractions are strong enough, then the filler attraction plus matrix-induced depletion effects can induce macroscopic phase separation into matrix rich and tethered nanoparticle rich coexisting phases. (iii) If nanoparticle−nanoparticle attractions are strong enough relative to the thermal energy, and sufficient steric stabilization exists due to tether repulsion to preclude macrophase demixing, then stable aggregate formation and/or microphase type of ordering can occur. All three types of behavior are found for attractive tethered nanoparticles as described in section IV. The competing physical effects that determine the thermodynamics and structure are functions of chemistry (via nanoparticle attraction strength), tether grafting density and chain length, matrix chain length, total packing fraction, and mixture composition.

PRISM theory describes correlated and spatially segregated, but globally homogeneous, fluid states. It is not a mean field theory and includes concentration fluctuations on all length scales. Hence, literal spinodal instabilities at nonzero wave vectors (structure factor divergences at k^*) are not predicted.[39-43] However, in extensive prior applications of the theory to diblock[27,39-43] and multiblock[48,49] copolymers, an analysis of small angle scattering profiles was proposed which allows a useful estimate of a microphase separation transition in the sense of an extrapolated spinodal instability. In polymer (mean) field theories and experimental scattering analyses, the quantity $1/S_{cc}(k^*)$ is taken as the order parameter which would vanish at a literal spinodal instability.[28,50] We estimate the spinodal instability via linear extrapolation of $1/S_{cc}(k^*)$ as a function of the inverse dimensionless temperature, $1/T^*$. When applied to melts of single-tethered particles,[24] the resulting microphase spinodal curve was in good agreement with the order−disorder boundary obtained using simulations by Iacovella et al.[21] This prior work motivates an analogous analysis of the tethered particles in polymer matrix system.

A schematic of the microphase spinodal temperatures, T^*, versus total packing fraction, η, and volume fraction of tethered particles, ϕ, phase diagram is shown in Figure 1b. In previous work,[24,25] a power law dependence of T^* (solid lines) on η for melts of tethered particles ($\phi = 1$) was found for all values of number of tethers, with an effective scaling exponent much smaller than that for diblock copolymers. Our primary present aim is to study how the microphase spinodal curves (dashed lines) change upon addition of polymer matrix (decreasing ϕ), as schematically indicated in Figure 1b.

D. System Parameters. There are many controllable material parameters: tether degree of polymerization, N_p, number of tethers, f, placement of tethers, ratio of particle-to-monomer diameter, D/d, matrix polymer degree of polymerization, N_m, total fluid packing fraction, η, fraction of η composed of tethered particles, ϕ, and absolute magnitude of the particle−particle attraction strength in units of the thermal energy, ε_{cc}. Most calculations are for tethered particles with $N_p = 8$ and 27, $f = 1$ and 2, and $D/d = 2$ and 3, and polymer matrix lengths ranging from $N_m = 1$("solvent") to 50. For the two-tethered nanoparticles, the grafted chains are placed 180° apart. We also present a few results for $f = 6$ where the tethers
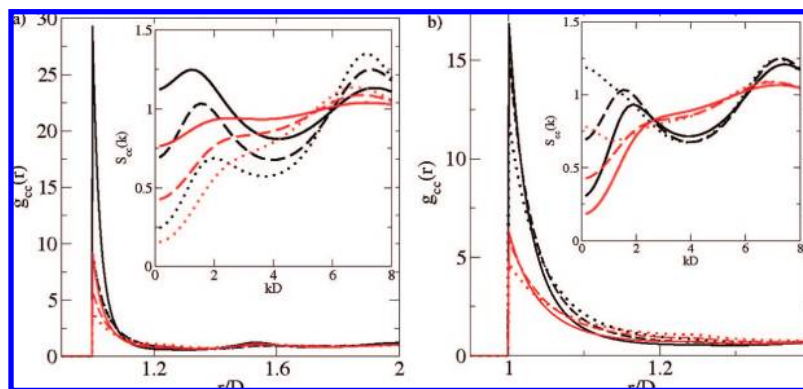
Figure 2. Particle−particle pair correlation function, $g_{cc}(r)$, and collective structure factor, $S_{cc}(k)$, as inset, for nanoparticles under athermal conditions with 1 (black) and 2 (red) tethers of $N_p = 8$, particle size $D/d = 2$, in a matrix of variable polymer of degree of polymerization: (a) $N_m = 8$ at a packing fraction $\eta = 0.5$, $\phi = 0.2$ (solid), 0.5 (dashed), 0.8 (dotted) and (b) $N_m = 1$ (solid), 8 (dashed), and 50 (dotted) at a packing fraction $\eta = 0.5$, $\phi = 0.5$.

are placed symmetrically on the filler surface. In all cases, the attachment points are fixed corresponding to a "quenched" (not annealed) grafting process. The consequences of variable tether placement on structure and phase behavior of tethered nanoparticles in the absence of free homopolymer has been discussed in ref 25. The attraction strength ε_{cc} is varied from 0 (athermal) to several kT. The total packing fraction, η, is varied from 0.3−0.5, representative of a dense melt.

In section III, we present results for a purely entropic (athermal) system of $f = 1$ and 2 tethered nanoparticles in a polymer matrix. Section IV explores the effect of interparticle attraction strength, number of tethers ($f = 1$, 2, and 6), matrix polymer length, particle size, and tether chain length on filler dispersion, and microphase and macrophase spinodals. Although PRISM theory provides all six distinct $g_{ij}(r)$ and partial structure factors, $S_{ij}(k)$, we focus entirely on the nanoparticle−nanoparticle correlations, $g_{cc}(r)$ and $S_{cc}(k)$.

III. Athermal Limit

The particle−particle pair correlation function, $g_{cc}(r)$, and collective structure factor, $S_{cc}(k)$, provide a statistical picture of the spatial organization of the polymer-tethered nanoparticles in the polymer matrix. In Figure 2a, we present these quantities for $D/d = 2$ with $f = 1$ and 2 tethers of length $N_p = 8$ in a $N_m = 8$ matrix at a packing fraction $\eta = 0.5$ for $\phi = 0.2$, 0.5, and 0.8. For all compositions, as the number of tethers increases from 1 to 2, $g_{cc}(r)$ at contact decreases. The presence of additional peaks at $r/D \sim 1.55$ and 2 suggest weak local ordering beyond contact. The structure factors for $f = 1$ systems have a weak small angle peak, which is absent for $\eta < 0.5$ (not shown), and two-tethered particles do not exhibit any small angle peak. All trends imply that as the number of tethers increases nanoparticle clustering is reduced because of enhanced steric repulsion. For both $f = 1$ and 2, as ϕ decreases from 0.5 (dotted curve) to 0.2 (solid curve), $g_{cc}(r)$ at contact and the magnitude of the small angle peak increase. This is because, as the fraction of polymer matrix increases, the tethered particles are entropically pushed together due to matrix-induced depletion attraction.

The effect of matrix polymer chain length on the organization of $f = 1$ and 2 tethered particles is shown in Figure 2b for tether length $N_p = 8$ and $N_m = 1$, 8, and 50, at fixed $\eta = 0.5$, $\phi = 0.5$. The local particle order is not very sensitive to N_m under athermal conditions, although the contact values of $g_{cc}(r)$ weakly decrease as N_m increases. Interestingly, this trend is opposite that found in the case of the homopolymer matrix containing relatively large nanoparticles with high surface grafting density.[5] The reason is presumably that classic polymer brush physics is relevant at high graft densities under locally flat surface ($D/d \gg 1$) conditions where filler dispersion is governed by entropic
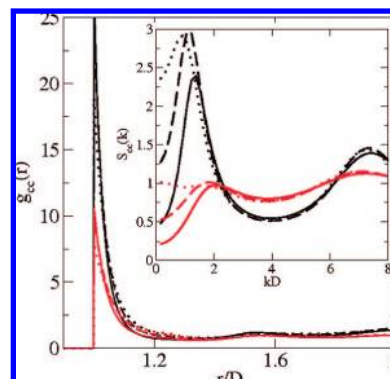
Figure 3. Particle−particle pair correlation function, $g_{cc}(r)$, and structure factor, $S_{cc}(k)$, for tethered nanoparticles with 1 (black) and 2 (red) tethers of $N_p = 8$, particle size $D/d = 2$, in a matrix polymer of degree of polymerization $N_m = 1$ (solid), 8 (dashed), and 50 (dotted) at a packing fraction $\eta = 0.5$, $\phi = 0.5$, and $\varepsilon_{cc} = kT$.

wettability considerations.[51−53] For nanoparticles with only one or two polymer tethers, dispersability is likely controlled by the fraction of a filler surface covered by grafted chains and unavailable for nanoparticle contacts.

The weak small angle peak in $S_{cc}(k)$ (inset of Figure 2b) for single-tethered particles decreases as N_m increases and disappears for $N_m = 50$. There are no small angle peaks for two-tethered nanoparticles. The nanoparticle osmotic compressibility, directly related to $S_{cc}(k = 0)$, grows as N_m increases for both 1 and 2 tether cases.

IV. Attractive Tethered Nanoparticle Fillers

We now study the effect of increasing nanoparticle−nanoparticle attraction strength on local structure and phase behavior. We remind the reader that a physical discussion of the "dilution" and "depletion" aspects of the microphase and macrophase spinodals discussed below was presented in section IIC.

A. Pair Correlation Functions and Structure Factors. In Figure 3, $g_{cc}(r)$ and $S_{cc}(k)$ of nanoparticles with 1 and 2 tethers of length $N_p = 8$ and particle size $D/d = 2$ in matrices of chain lengths $N_m = 1$, 8, and 50 at $\eta = 0.5$, $\phi = 0.5$ are presented for a relatively weak attraction strength $\varepsilon_{cc} = kT$. At fixed N_m, aggregation of the tethered particles decreases as f increases, similar to athermal limit results in Figure 2b. For both $f = 1$ and 2, the local ordering is similar, with no major effect of matrix polymer chain length on either structure. In the inset of Figure 3, the single-tethered particles exhibit a much stronger small angle peak in $S_{cc}(k)$ than two-tethered particles for all
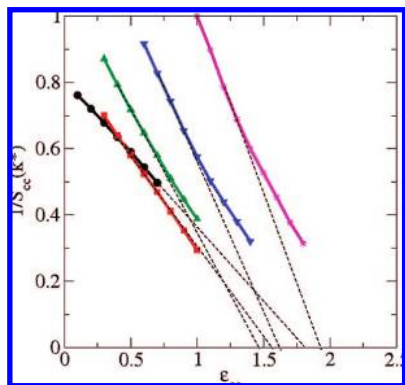
Figure 4. Inverse of the microphase order parameter, $1/S_{cc}(k^*)$, as a function of particle attraction strength in units of the thermal energy, ε_{cc}, for single-tethered particles of size $D/d = 2$ with tether length $N_p = 8$ in a polymer matrix of length 8 at $\eta = 0.5$ and $\phi = 0.2$ (circle), 0.4 (square), 0.6 (up triangle), 0.8 (down triangle), and 1.0 (star). Dashed lines show the linear extrapolation employed to obtain spinodal attraction strengths (ε^*_{cc}).

matrix polymer lengths. In addition, for $f = 1$, the small angle peak is higher for the intermediate value of $N_m = 8$ compared with $N_m = 1$ and 50. This nonmonotonicity, only seen for $f = 1$, is further discussed in the next section. For both $f = 1$ and 2, $S_{cc}(k = 0)$ grows as N_m increases similar to athermal limit results (Figure 2b).

B. Apparent Microphase Spinodal Curves. We expect that microphase separation is induced primarily via clustering of nanoparticles, as schematically illustrated in Figure 1a, a signature of which is the emergence of a prominent small angle peak in $S_{cc}(k)$. In contrast, we find (not shown) only a weak small angle peak in the tether collective structure factor, $S_{pp}(k)$, and in the matrix polymer structure factor, $S_{mm}(k)$, for $\phi > 0.6$, and no peaks in $S_{pp}(k)$ or $S_{mm}(k)$ for $\phi < 0.6$. These differences reflect the large asymmetry of collective concentration fluctuations of the different species due to excluded volume and packing considerations, and nonzero mixture compressibility, in contrast with the essentially incompressible block copolymer melt.[50] Hence, $S_{cc}(k^*)$ is employed as the order parameter to estimate microphase separation spinodal temperatures. In Figure 4, $1/S_{cc}(k^*)$ is plotted as a function of particle−particle attraction strength, ε_{cc}, for single-tethered particles of size $D/d = 2$, tether length $N_p = 8$, in a polymer matrix of length $N_m = 8$, at $\eta = 0.5$ and varying ϕ. Dashed lines show the linear extrapolation utilized to obtain spinodal attraction strengths (ε^*_{cc}).

In Figure 5a, the deduced microphase spinodal temperature T^* ($= 1/\varepsilon^*_{cc}$) is presented as a function of ϕ for $f = 1$, $D/d = 2$, $N_p = 8$ fillers at $\eta = 0.5$ and $\eta = 0.3$, and varying matrix polymer length. For all N_m, the shape of the spinodal curve for $\eta = 0.5$ (solid curves) exhibits a competition between dilution (T^* decreases as ϕ decreases) and depletion (T^* increases as ϕ decreases) behavior. For single tethered particles, the steric hindrance due to the intertether repulsion is minimized, and nanoparticles can form enthalpic contacts that are further favored via the depletion-like attractions mediated by matrix polymers as occurs in bare nanoparticle−polymer mixtures.[34,35] Note also that for $\eta = 0.5$ as the matrix polymer length increases the spinodal temperature varies nonmonotonically for most ϕ. When $0.2 \leq \phi \leq 0.6$, as N_m increases from 1 to 4, the microphase spinodal temperature increases, but as N_m increases from 4 to 50, we find T^* decreases with the highest value attained for $N_m = 4$. When $\phi < 0.2$ (system consisting of mostly polymer matrix), T^* decreases monotonically with increasing N_m. When $\phi > 0.6$ (system consisting of mostly tethered particles), the trend is not clear since the T^* does not vary much with N_m.

At a packing fraction of $\eta = 0.4$ (not shown), there is a slight change in shape of the spinodal curves, shifting toward dilution-like behavior, while the nonmonotonicity continues to exist. The value of N_m at which T^* is highest is different from that for $\eta = 0.5$. At high ϕ (>0.8), the effect of N_m is minimal since there is not much matrix polymer present. At intermediate ϕ ($0.4 \leq \phi \leq 0.7$) when N_m increases from 1 to 8, we find T^* increases, but for $N_m > 8$, the spinodal temperature decreases with its highest value achieved for $N_m = 8$. At low ϕ (<0.3), macrophase separation occurs, and thus there is no clear trend for T^* with varying N_m. We note that the spinodal macrophase separation transition is determined by the simultaneous divergence of all partial collective structure factors at zero wavevector, that is, $S_{ij}(k = 0) \rightarrow \infty$ or equivalently $\Lambda(k = 0) \rightarrow 0$ in eq A9 in the Appendix.

At a lower packing fraction of $\eta = 0.3$ (dashed lines in Figure 5a), the shape of the spinodal curves become more dilution-like, and the microphase spinodal temperature decreases. The nonmonotonic behavior, with T^* being highest for an intermediate N_m, is still present at $\eta = 0.3$. For clarity of presentation, the $N_m = 4$ and 25 results are not shown since the nonmonotonic dependence of T^* on N_m is apparent from the $N_m = 1$, 8, and 50 results. Overall, we conclude that for single-tethered particles in polymer matrix there is a rich competition between depletion and dilution effects.

C. Mean Field-Like Limits. In order to better understand the origin of the interesting nonmonotonic behavior in Figure 5a and make contact with the classic block copolymer theory of microphase separation,[50] we calculate the spinodal T^* using mean-field-like approximations (or "random phase approximation", RPA) within a liquid state theory framework. Unlike the incompressible mean field theory for block copolymers,[50] in the PRISM framework a "RPA" does include liquid compressibility effects and local correlations,[27,54] in the spirit of a nonself-consistent mean spherical approximation (MSA) closure of the Ornstein−Zernike integral equation theory.[45]

Technically, the liquid state RPA implies an additive structure for the direct correction function, which plays the role of an effective pair potential[27,45,54]

$$C_{ij}(k) = C_{ij}^{(0)}(k) + \Delta C_{ij}(k) \qquad (6)$$

where beyond the distance of closest approach:

$$\Delta C_{ij}(r) = -\beta U_{ij}(r) \quad \text{(MSA)} \qquad (7)$$

$$\Delta C_{ij}(r) \approx -\beta U_{ij}(r) g_{ij}^{(0)}(r) \quad \text{(MPY/HTA)} \qquad (8)$$

Here, C_{ij} is the direct correlation function between species i and j; $C_{ij}^{(0)}$ is the corresponding athermal limit; $U_{ij}(r)$ is the (noncontact) potential between species i and j, and $g_{ij}^{(0)}(r)$ is the athermal pair correlation function. Equation 6 neglects the coupling between repulsive and attractive interactions on the direct correlations, which is required on the local scale to rigorously enforce excluded volume constraints. It also neglects long-range concentration fluctuations, which destroy the spinodal of a first order transition such as microphase separation via coupling of local and macromolecular scale correlations.[39,41−43,55] Equation 8 corrects the MSA for nonrandom local packing correlations in the athermal reference system, as suggested by molecular closure analysis for polymer mixtures.[27,54] A literal microphase spinodal temperature does exist based on eqs 6−8 in the PRISM formalism.[27,54] For the system of present interest, it is found by determining the value of ε_{cc} for which all of the partial structure factors simultaneously first diverge at a nonzero wave vector (see Appendix).

Mean-field-like microphase spinodal results are presented in Figure 5b. As expected, the values of T^* are not the same as those deduced based on full PRISM calculations (Figure 5a). Spinodal temperatures computed using eq 7 are in the same
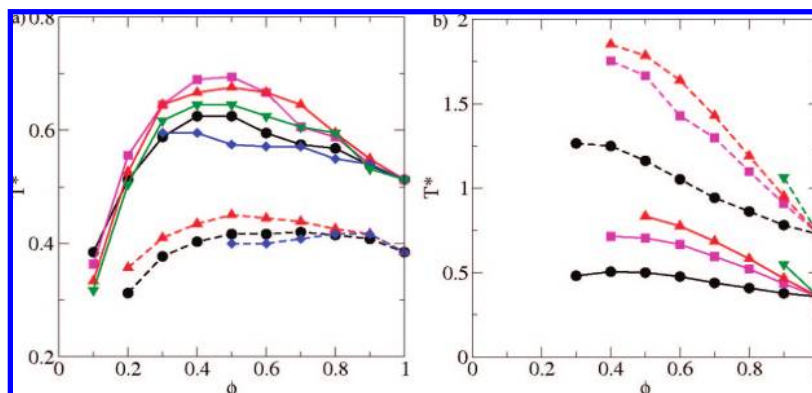
Figure 5. Microphase spinodal temperature, T^* ($=1/\varepsilon^*_{cc}$) as a function of mixture composition, ϕ, for single-tethered particles of size $D/d = 2$ with tether length $N_p = 8$ in a polymer matrix of length $N_m = 1$ (circle), 4 (square), 8 (up triangle), 25 (down triangle), and 50 (diamond) for (a) $\eta = 0.5$ (solid) and $\eta = 0.3$ (dashed) using the full PRISM theory (for clarity, the $N_m = 4$ and 25 calculations for $\eta = 0.3$ are omitted) and (b) at $\eta = 0.5$ based on the mean-field-like approximations of eq 7 (solid) and eq 8 (dashed). Results for $N_m = 50$ are not shown since no microphase separation spinodal transition was found for most mixture compositions ($0.1 < \phi < 0.9$).
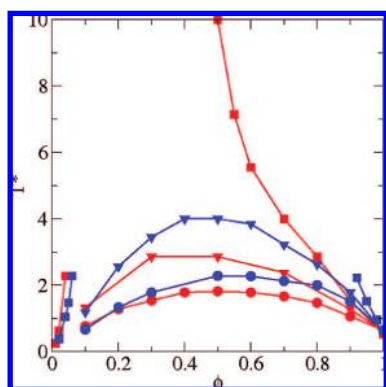
Figure 6. Macrophase separation spinodal temperature as a function of mixture composition for bare particles of size $D/d = 2$ in a polymer matrix of length 8 (red) and 50 (blue) at total fluid packing fractions $\eta = 0.4$ (square), 0.35 (triangle), and 0.3 (circle).

range as full PRISM analogs, while the T^* values calculated using eq 8 are higher than full PRISM calculations. Most importantly, there are qualitative differences. For example, at $\eta = 0.5$, T^* increases as ϕ decreases in the range $0.5 < \phi < 1.0$ in both mean-field-like approaches, in contrast to the results in Figure 5a. Also, the mean field T^* do not exhibit any nonmonotonic behavior with increasing matrix polymer length N_m. This suggests the latter subtle behavior predicted by the full PRISM theory is primarily due to changes of local packing of the particle and tethers with increasing ε_{cc} which is sensitive to matrix chain length.

It is of interest to contrast our results with those of analogous bare nanoparticle systems, which undergo macrophase demixing. Questions such as the temperature scale, role of matrix chain length, and form of the spinodal curve are of interest. For bare fillers, nanoparticle–nanoparticle attractions and entropically mediated depletion attractions reinforce each other resulting in poor filler dispersability.[34−36] Figure 6 shows representative macrophase separation results determined numerically using the full PRISM theory via the condition $S^{-1}_{ij}(k = 0) = 0$. The nonmonotonic behavior with varying N_m (seen in Figure 5a) is not seen for bare nanoparticles in a polymer matrix, and the macrophase spinodal temperatures are much higher than the analogous microphase spinodal temperatures of single-tethered particles at the same packing fraction. For example, at $\eta = 0.3$ the macrophase T^* for bare fillers is ∼1−2 (Figure 6), while the microphase T^* for single tethered particle is ∼0.2−0.4 (Figure 5a). At all ϕ, the macrophase T^* increases with N_m, suggesting

that the nonmonotonic trend with N_m is unique to single-tethered particles.

D. Effect of Number of Tethers on the Phase Behavior. The effect of number of tethers ($f = 1$, 2, and 6) on the microphase spinodal is shown in Figure 7a for nanoparticles of size $D/d = 2$, tether length $N_p = 8$, at $\eta = 0.5$. For the $f = 6$ system, the six tethers are placed symmetrically on the nanosphere. As f increases, T^* decreases due to enhanced steric shielding of nanoparticle close contacts (also seen for a melt of tethered particles[24,25]), the effect of matrix length N_m on T^* diminishes, and a strikingly more dilution-like behavior occurs.

Figure 7b,c presents the analogous mean-field-like results for one- and two-tethered nanoparticles. For $f = 1$, both mean-field calculations predict the same shape of the spinodal curve found based on the full PRISM calculation (Figure 7a). However, for $f = 2$ the dependence of T^* on ϕ is qualitatively different; in the mean-field calculation, T^* weakly increases as ϕ decreases, while in full PRISM theory T^* decreases as ϕ is lowered, indicating a dilution-type behavior. The fact that the mean-field-like calculations do not predict dilution-like behavior with increasing number of tethers suggests its origin is coupled energetic/packing effects on the local structure of the nanoparticles that depends on interparticle attraction strength.

E. Effect of Particle Size and Tether Length. Figure 8a presents microphase spinodal curves for a larger nanoparticle of $D/d = 3$ with a single tether of length $N_p = 27$ and 8 in a polymer matrix of varying chain length at $\eta = 0.4$. We have chosen $N_p = 27$ so that the total volume of a single tether equals the nanoparticle volume. This allows a fair comparison to be made with the smaller $N_p = 8$ and $D/d = 2$ nanoparticle system under the same equal space-filling volume condition. The shape of the microphase spinodal curve for $N_p = 27$ and $D/d = 3$ (solid curves) is similar to that for $N_p = 8$ and $D/d = 2$ at $\eta = 0.4$ (not shown). The microphase spinodal temperatures are slightly higher for $D/d = 3$ at all compositions. Unlike the smaller single-tethered particle which exhibited a nonmonotonic dependence of T^* on matrix polymer length, the value of N_m does not have any effect on the spinodal temperatures for the larger single-tethered particles. However, by simply decreasing the tether length from $N_p = 27$ to $N_p = 8$, while maintaining constant particle size at $D/d = 3$ (dashed curves in Figure 8a), the shape of the spinodal curves are completely changed. We observe macrophase separation at all $\phi < 0.6$ for matrix polymer length $N_m = 4$, at all $\phi < 0.8$ for $N_m = 8$, and at all $\phi < 0.9$ for $N_m = 25$. Thus, the range of compositions where macrophase separation occurs significantly increases with matrix polymer length.
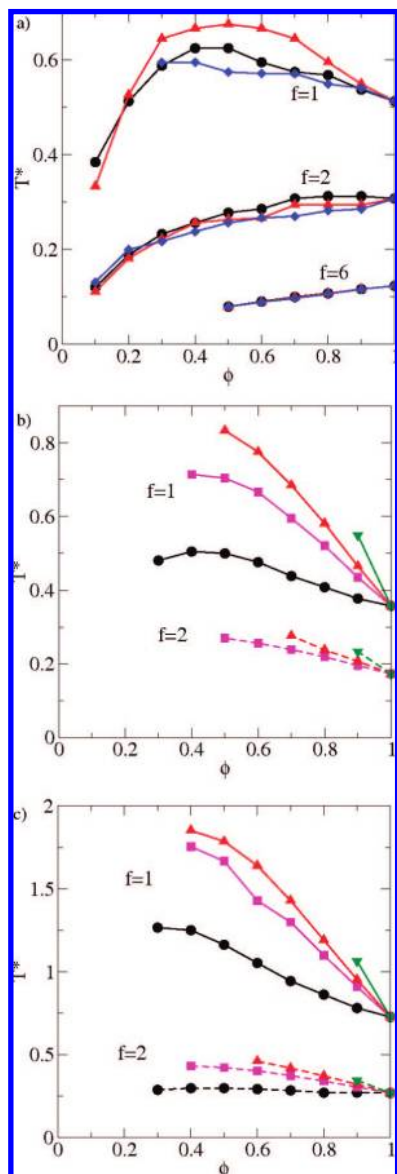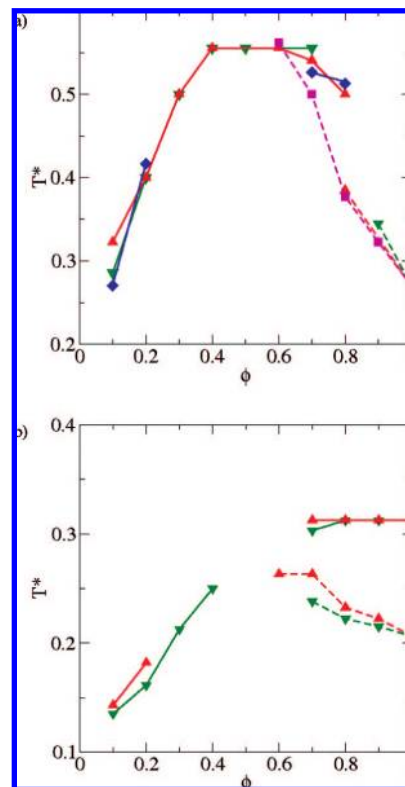
Figure 7. (a) Microphase spinodal temperature as a function of mixture composition for tethered particles of size $D/d = 2$, with $f = 1$, 2, and 6 tethers of length $N_p = 8$ in a polymer matrix of length 1 (circle), 8 (up triangle), and 50 (diamond) at a packing fraction $\eta = 0.5$. Mean field microphase spinodal curves for 1- and 2-tethered particles of size $D/d = 2$ and tether length $N_p = 8$ in a polymer matrix of length 1 (circle), 4 (square), 8 (up triangle), and 25 (down triangle) at $\eta = 0.5$ are shown based on (b) eq 7 and (c) eq 8.

The results in Figure 8a suggest that, for single tethered particles in a polymer melt with fixed chain length, as the tether length is decreased ($N_p = 27$ to 8) at a constant particle size ($D/d = 3$), or the particle size is increased ($D/d = 2$ to 3) at a constant tether length ($N_p = 8$), the tendency for macrophase separation increases. In our previous work[24] on melts of single-tethered particles, a similar trend of increasing macrophase separation with increasing particle size at constant tether length was found. This trend occurs because as the nanoparticle volume becomes much larger than the tether volume, the effectiveness of grafted chains in promoting dispersion diminishes and macrophase separation is favored. The presence of a homopolymer matrix enhances this macrophase separation tendency via the entropic depletion-like attraction.

Figure 8b presents analogous results for two-tethered particles. The shape of the microphase spinodal curves is again completely changed by simply decreasing the tether length from $N_p = 27$

Figure 8. Microphase spinodal temperature as a function of mixture composition for tethered particles of size $D/d = 3$ with (a) one tether of length $N_p = 27$ (solid) in a polymer matrix of length $N_m = 8$ (up triangle), 27 (down triangle), and 50 (diamond) and one tether of length $N_p = 8$ (dashed) in a polymer matrix of length $N_m = 4$ (square), 8 (up triangle), and 25 (down triangle) and (b) two tethers of length $N_p = 27$ (solid) in a polymer matrix of length 8 (up triangle) and 27 (down triangle) and $N_p = 8$ (dashed) in a polymer matrix of length 8 (up triangle) and 25 (down triangle).

(solid lines) to $N_p = 8$ (dashed lines) when $D/d = 3$. The gaps in the spinodal curves, especially at $0.3 < \phi < 0.7$, occur since we were unable to numerically converge the integral equations to an extent that allows calculation of the spinodal temperatures at those compositions. An interesting feature in Figure 8b is that the change in T^* with decreasing N_p is smaller for the two tether particles compared with the $f = 1$ analogs. This suggests that increasing the number of tethers reduces the effect of particle size and tether length on the microphase spinodal curves.

V. Summary and Discussion

We have extended and applied PRISM theory to study the structural correlations and phase behavior of spherical nanoparticles with a modest number of tethered chains dissolved in a homopolymer matrix under dense melt conditions. Only particle–particle interactions are attractive. For melts and dense solutions of one-, two-, and four-tethered nanoparticles,[24,25] we previously discovered a power law dependence of the microphase spinodal temperature, T^*, on packing fraction η with an exponent much smaller than that for diblock copolymers.[40,56] In the presence of a polymer matrix, grafted chain and attractive nanoparticles experience clustering and/or microphase separation determined by a competition between tether repulsion and interparticle attraction, and depletion-like macrophase separation induced by the polymer matrix. Overall, a rich and subtle competition between dilution-like and depletion-like effects on the structural organization emerges depending on system parameters and hybrid filler architecture.

Calculations of the particle–particle pair correlation functions, $g_{cc}(r)$, and collective structure factors, $S_{cc}(k)$, of single- and two-tethered particles, under both athermal entropic conditions and in the presence of filler attractions, suggest that as number of tethers increases nanoparticle clustering decreases. A plot of the inverse of the microphase order parameter, $1/S_{cc}(k^*)$, as a function of particle attraction strength, ε_{cc} (in units of kT), was employed to obtain an extrapolated microphase spinodal temperature. For single-tethered nanoparticles with $D/d = 2$ and tether length $N_p = 8$ in a homopolymer matrix of length $N_m = 8$, the shape of the microphase spinodal curve is a combination of dilution-like and depletion-like behavior, and shows a nonmonotonic dependence on varying matrix polymer length for $\eta = 0.3-0.5$. This nonmonotonicity is absent in mean-field-like calculations, which ignore the coupling of repulsive and attractive interactions on a local scale and longer wavelength concentration fluctuations. This suggests that short-range structure plays a major role in the nonmonotonic microphase ordering scale behavior via a coupling of local and macromolecular correlations.[27,39–43] As the number of tethers is increased from one to six, the microphase spinodal curves become more dilution-like, and the matrix polymer length no longer affects the spinodal temperature. The reason for the former trend is that as the number of tethers grows there is enhanced shielding of the nanoparticle surface which precludes close contacts.

For single tether fillers of fixed tether length, as the nanoparticle size is increased the tendency for macrophase separation increases, and more so for longer matrix chains. This occurs because as nanoparticle volume exceeds tether volume the ability of the grafted chain to promote steric stabilization diminishes. When the particle size and tether length are both increased, such that the total volume of tethered monomers and nanoparticle volume are equal, the shape of the microphase spinodal curve remains unchanged, but the sensitivity to matrix polymer length diminishes. As the number of tethers increases, the effect of particle size and tether length on the microphase spinodal temperatures also decreases.

We note that ignoring the nonideal conformational effects in this work, although a reasonable first approximation at high melt-like volume fractions in the absence of all matrix polymer and tether polymer attractive interactions, could potentially bias the predicted local structure in these systems. Unfortunately, the present lack of experimental and simulation results for single- and two-tethered particles dissolved in a dense polymer melt precludes critically testing our theory. There are preliminary experiments on six-tethered particles (albeit with larger nanoparticles) in a homopolymer melt by Kumar and co-workers,[57] and a detailed PRISM study of this system will be presented in a future publication. We are also not aware of any liquid state theory based density functional study of microphase separation, and to date self-consistent field theory has only been applied to melts of single tether "tadpoles" in the absence of free homopolymer.[23] Finally, our approach is not only applicable to spherical tethered particles in a homopolymer matrix, but can also treat physical and chemical heterogeneities of nanoparticles (e.g., nonspherical fillers) and/or matrix (e.g., blends, block copolymers).

Appendix

We summarize the key equations for the intramolecular structure factors of the hybrid tethered nanoparticle, $\omega_{ij}(k)$, total intermolecular structure factors, $h_{ij}(k)$, and partial collective structure factors, $S_{ij}(k)$, used in the PRISM calculations.

The intramolecular structure factors for the particle–particle, tether-particle and tether-tether are

$$\omega_{cc}(k) = 1 \tag{A1}$$

$$\omega_{pc}(k) = \frac{f}{Nf+1} \sum_{\alpha=1}^{N} \left[\frac{\sin(kl)}{kl}\right]^{|\alpha-1|} \frac{\sin(kR)}{kR} \tag{A2}$$

$$\omega_{pp}(k) = \frac{f}{Nf}\left[\sum_{\alpha_i}^{N}\sum_{\gamma_i}^{N}\left[\frac{\sin(kl)}{kl}\right]^{|\alpha_i-\gamma_i|} + \right.$$
$$\left. (f-1)\sum_{\alpha_i}^{N}\sum_{\gamma_j}^{N}\left[\frac{\sin(kl)}{kl}\right]^{|\alpha_i-1|} \times \left[\frac{\sin(kl)}{kl}\right]^{|\gamma_j-1|} T(k)\right] \tag{A3}$$

where for two tethers placed at $180°$ is $T(k) = \sin(2kR)/2kR$. The matrix polymer intramolecular structure factor is

$$\omega_{mm}(k) = \frac{\left[1 - \left(\frac{\sin(kl)}{kl}\right)^2 - 2N_m^{-1}\frac{\sin(kl)}{kl} + 2N_m^{-1}\left(\frac{\sin(kl)}{kl}\right)^{N_m+1}\right]}{\left(1 - \frac{\sin(kl)}{kl}\right)^2} \tag{A4}$$

The equations for $h_{ij}(k)$, for any three species two-component system containing an AB molecule in C "solvent" are (A denotes tether, B is nanoparticle, and C is matrix polymer)

$$\Lambda h_{AA} = (1 - \rho_C\omega_{CC}C_{CC})\{-\rho_B\omega_{AA}\delta\omega\delta C + \omega_{AA}^2 C_{AA} + f_A^{-2}\omega_{AB}^2 C_{BB} +$$
$$2f_A^{-1}\omega_{AA}\omega_{AB}C_{AB}\} + \rho_C\omega_{CC}\{\rho_B\omega_{AA}\delta\omega\delta C_{ABC} + \omega_{AA}^2 C_{AC}^2 +$$
$$f_A^{-2}\omega_{AB}^2 C_{BC}^2 + 2f_A^{-1}\omega_{AA}\omega_{AB}C_{AC}C_{BC}\} \tag{A5}$$

$$\Lambda h_{AC} = \omega_{CC}\{C_{AC}\omega_{AA} + f_A^{-1}C_{BC}\omega_{AB} + \rho_B\delta\omega(C_{AB}C_{BC} - C_{BB}C_{AC})\} \tag{A6}$$

and Λh_{BB} and Λh_{BC} follow by interchanging the A and B labels

$$\Lambda h_{AB} = (1 - \rho_C\omega_C C_{CC})\{-\rho_m\omega_{AB}\delta\omega\delta C + C_{AB}(\omega_{AA}\omega_{BB} + f_A^{-1}f_B^{-1}\omega_{AB}^2) + \omega_{AB}(f_B^{-1}\omega_{AA}C_{AA} + f_A^{-1}\omega_{BB}C_{BB})\} +$$
$$\rho_C\omega_{CC}\{C_{AC}C_{BC}(\omega_{AA}\omega_{BB} + f_A^{-1}f_B^{-1}\omega_{AB}^2) + \omega_{AB}(f_B^{-1}\omega_{AA}C_{AC}^2 + f_A^{-1}\omega_{BB}C_{BC}^2) + \rho_m\omega_{AB}\delta\omega\delta C_{ABC}\} \tag{A7}$$

$$\Lambda h_{CC} = \omega_{CC}^2\{\rho_A\rho_B\delta\omega\delta C_{ABC} + \rho_A\rho_B C_{CC}\delta\omega\delta C + C_{CC}(1 - \rho_A\omega_{AA}C_{AA} - \rho_B\omega_{BB}C_{BB} - 2\rho_m\omega_{AB}C_{AB}) +$$
$$2\rho_m\omega_{AB}C_{AC}C_{BC} + \rho_A\omega_{AA}C_{AC}^2 + \rho_B\omega_{BB}C_{BC}^2\} \tag{A8}$$

where

$$\Lambda(k) = 1 - \rho_A\omega_{AA}C_{AA} - \rho_B\omega_{BB}C_{BB} - 2\rho_m\omega_{AB}C_{AB} +$$
$$\rho_A\rho_B\delta\omega\{(1 - \rho_C\omega_{CC}C_{CC})\delta C - \rho_C\omega_{CC}\delta C_{ABC}\} -$$
$$\rho_C\omega_{CC}C_{CC} + 2\rho_m\rho_C\omega_{AB}\omega_{CC}(C_{AB}C_{CC} - C_{AC}C_{BC}) +$$
$$\rho_A\rho_C\omega_{AA}\omega_{CC}(C_{AA}C_{CC} - C_{AC}^2) +$$
$$\rho_B\rho_C\omega_{BB}\omega_{CC}(C_{BB}C_{CC} - C_{BC}^2) \tag{A9}$$

$$\delta\omega = \omega_{AA}\omega_{BB} - f_A^{-1}f_B^{-1}\omega_{AB}^2$$
$$\delta C = C_{AA}C_{BB} - C_{AB}^2$$
$$\delta C_{ABC} = 2C_{AB}C_{BC}C_{AC} - C_{AA}C_{BC}^2 - C_{BB}C_{AC}^2$$

and $\rho_m = \rho_A + \rho_B$

The corresponding partial collective structure factors are

$$\Lambda S_{AA} = \{\rho_A\omega_{AA}(1 - \rho_C\omega_{CC}C_{CC}) - \rho_A\rho_B\delta\omega(C_{BB} - \rho_C\omega_{CC}C_{CC}C_{BB} + \rho_C\omega_{CC}C_{BC}^2)\} \tag{A10}$$

$$\Lambda S_{AC} = \rho_C \omega_{CC} \{ \rho_A \omega_{AA} C_{AC} + \rho_m \omega_{AB} C_{BC} + \\ \rho_A \rho_B \delta\omega (C_{AB} C_{BC} - C_{BB} C_{AC}) \} \quad (A11)$$

S_{BB} and S_{BC} can be obtained by interchanging A and B labels,

$$\Lambda S_{AB} = \{ \rho_m \omega_{AB} (1 - \rho_C \omega_{CC} C_{CC}) + \\ \rho_A \rho_B \delta\omega (C_{AB} - \rho_C \omega_{CC} C_{CC} C_{AB} + \rho_C \omega_{CC} C_{AC} C_{BC}) \} \quad (A12)$$

$$\Lambda S_{CC} = \rho_C \omega_{CC} \{ 1 - \rho_A \omega_{AA} C_{AA} - \rho_B \omega_{BB} C_{BB} - 2\rho_m \omega_{AB} C_{AB} + \\ \rho_A \rho_B \delta\omega \delta C \} \quad (A13)$$

References and Notes

(1) Krishnamoorti, R.; Vaia, R. A. *J. Polym. Sci., Part B: Polym. Phys.* **2007**, *45*, 3252–3256.

(2) Winey, K. I.; Vaia, R. A. *MRS Bull.* **2007**, *32*, 314–319.

(3) Harton, S. E.; Kumar, S. K. *J. Polym. Sci., Part B: Polym. Phys.* **2008**, *46*, 351–358.

(4) Corbierre, M. K.; Cameron, N. S.; Sutton, M.; Laaziri, K.; Lennox, R. B. *Langmuir* **2005**, *21*, 6063–6072.

(5) Lan, Q.; Francis, L. F.; Bates, F. S. *J. Polym. Sci., Part B: Polym. Phys.* **2007**, *45*, 2284–2299.

(6) Glogowski, E.; Tangirala, R.; Russell, T. P.; Emrick, T. *J. Polym. Sci., Part A: Polym. Chem.* **2006**, *44*, 5076–5086.

(7) Krishnamoorti, R. *MRS Bull.* **2007**, *32*, 341–347.

(8) Causin, V.; Yang, B. X.; Marega, C.; Goh, S. H.; Marigo, A. *J. Nanosci. Nanotechnol.* **2008**, *8*, 1790–1796.

(9) Tsubokawa, N. *Polym. J.* **2007**, *39*, 983–1000.

(10) Goel, V.; Chatterjee, T.; Bombalski, L.; Yurekli, K.; Matyjaszewski, K.; Krishnamoorti, R. *J. Polym. Sci., Part B: Polym. Phys.* **2006**, *44*, 2014–2023.

(11) Currie, E. P. K.; Norde, W.; Stuart, M. A. C. *Adv. Colloid Interface Sci.* **2003**, *100*, 205–265.

(12) Westenhoff, S.; Kotov, N. A. *J. Am. Chem. Soc.* **2002**, *124*, 2448–2449.

(13) Song, T.; Dai, S.; Tam, K. C.; Lee, S. Y.; Goh, S. H. *Polymer* **2003**, *44*, 2529–2536.

(14) Song, T.; Dai, S.; Tam, K. C.; Lee, S. Y.; Goh, S. H. *Langmuir* **2003**, *19*, 4798–4803.

(15) Li, B.; Li, C. Y. *J. Am. Chem. Soc.* **2007**, *129*, 12–13.

(16) Kawauchi, T.; Kumaki, J.; Yashima, E. *J. Am. Chem. Soc.* **2005**, *127*, 9950–9951.

(17) Chan, E. R.; Ho, L. C.; Glotzer, S. C. *J. Chem. Phys.* **2006**, *125*, 064905.

(18) Chan, E. R.; Zhang, X.; Lee, C. Y.; Neurock, M.; Glotzer, S. C. *Macromolecules* **2005**, *38*, 6168–6180.

(19) Glotzer, S. C.; Horsch, M. A.; Iacovella, C. R.; Zhang, Z. L.; Chan, E. R.; Zhang, X. *Curr. Opin. Colloid Interface Sci.* **2005**, *10*, 287–295.

(20) Horsch, M. A.; Zhang, Z. L.; Glotzer, S. C. *Phys. Rev. Lett.* **2005**, *95*, 05615.

(21) Iacovella, C. R.; Keys, A. S.; Horsch, M. A.; Glotzer, S. C. *Phys. Rev. E* **2007**, *75*, 040801.

(22) Iacovella, C. R.; Horsch, M. A.; Zhang, Z.; Glotzer, S. C. *Langmuir* **2005**, *21*, 9488–9494.

(23) Lee, J. Y.; Balazs, A. C.; Thompson, R. B.; Hill, R. M. *Macromolecules* **2004**, *37*, 3536–3539.

(24) Jayaraman, A.; Schweizer, K. S. *J. Chem. Phys.* **2008**, *128*, 164904.

(25) Jayaraman, A.; Schweizer, K. S. *Langmuir* **2008**, *24*, 11119.

(26) Schweizer, K. S.; Curro, J. G. *Adv. Polym. Sci.* **1994**, *116*, 319–377.

(27) Schweizer, K. S.; Curro, J. G. *Adv. Chem. Phys.* **1997**, *98*, 1–142.

(28) Bates, F. S.; Fredrickson, G. H. *Annu. Rev. Phys. Chem.* **1990**, *41*, 525–557.

(29) Matsen, M. W. *Macromolecules* **1995**, *28*, 5765–5773.

(30) Fredrickson, G. H.; Leibler, L. *Macromolecules* **1989**, *22*, 1238–1250.

(31) Fuchs, M.; Schweizer, K. S. *Europhys. Lett.* **2000**, *51*, 621–627.

(32) Asakura, S.; Oosawa, F. *J. Chem. Phys.* **1954**, *22*, 1255–1256.

(33) Henderson, D.; Duh, D. M.; Chu, X. L.; Wasan, D. *J. Colloid Interface Sci.* **1997**, *185*, 265–268.

(34) Hooper, J. B.; Schweizer, K. S.; Desai, T. G.; Koshy, R.; Keblinski, P. *J. Chem. Phys.* **2004**, *121*, 6986–6997.

(35) Hooper, J. B.; Schweizer, K. S. *Macromolecules* **2005**, *38*, 8858–8869.

(36) Hooper, J. B.; Schweizer, K. S. *Macromolecules* **2006**, *39*, 5133–5142.

(37) Hall, L. M.; Schweizer, K. S. *J. Chem. Phys.* **2008**, *128*, 234901.

(38) Chandler, D.; Andersen, H. C. *J. Chem. Phys.* **1972**, *57*, 1930.

(39) Guenza, M.; Schweizer, K. S. *J. Chem. Phys.* **1997**, *106*, 7391–7410.

(40) Guenza, M.; Schweizer, K. S. *Macromolecules* **1997**, *30*, 4205–4219.

(41) David, E. F.; Schweizer, K. S. *J. Chem. Phys.* **1994**, *100*, 7767–7783.

(42) David, E. F.; Schweizer, K. S. *J. Chem. Phys.* **1994**, *100*, 7784–7795.

(43) David, E. F.; Schweizer, K. S. *Macromolecules* **1997**, *30*, 5118–5132.

(44) Heine, D. R.; Grest, G. S.; Curro, J. G. *Advanced Computer Simulation Approaches for Soft Matter Sciences I* **2005**, *173*, 209–249.

(45) Hansen, J. P.; McDonald, I. R. *Theory of Simple Liquids*; Academic: London, **1986**.

(46) Hindmarsh, A. C.; Brown, P. N.; Grant, K. E.; Lee, S. L.; Serban, R.; Shumaker, D. E.; Woodward, C. S. *ACM Transactions on Mathematical Software* **2005**, *31*, 363–396.

(47) Starr, F. W.; Douglas, J. F.; Glotzer, S. C. *J. Chem. Phys.* **2003**, *119*, 1777–1788.

(48) Kolbet, K. A.; Schweizer, K. S. *Macromolecules* **2000**, *33*, 1443–1458.

(49) Kolbet, K. A.; Schweizer, K. S. *Macromolecules* **2000**, *33*, 1425–1442.

(50) Leibler, L. *Macromolecules* **1980**, *13*, 1602–1617.

(51) Wijmans, C. M.; Leermakers, F. A. M.; Fleer, G. J. *Langmuir* **1994**, *10*, 4514–4516.

(52) Shull, K. R. *J. Chem. Phys.* **1991**, *94*, 5723–5738.

(53) Witten, T. A.; Leibler, L.; Pincus, P. A. *Macromolecules* **1990**, *23*, 824–829.

(54) Schweizer, K. S. *Macromolecules* **1993**, *26*, 6033–6049.

(55) Fredrickson, G. H.; Helfand, E. *J. Chem. Phys.* **1988**, *89*, 5890–5897.

(56) Lodge, T. P.; Pan, C.; Jin, X.; Liu, Z.; Zhao, J.; Maurer, W. W.; Bates, F. S. *J. Polym. Sci., Part B: Polym. Phys.* **1995**, *33*, 2289–2293.

(57) Akcora, P.; Liu, H.; Kumar, S. K.; Li, Y.; Benicewicz, B. C.; Schadler, L. S.; Acehan, D.; Panagiotopoulos, A. Z.; Douglas, J. F., submitted, **2008**.